On Multi-User EXIT Chart Analysis Aided Turbo-Detected MBER Beamformer Designs

Shuang Tan, Sheng Chen, and Lajos Hanzo

Abstract— This paper studies the mutual information transfer characteristics of a novel iterative soft interference cancellation (SIC) aided beamforming receiver communicating over both additive white Gaussian noise (AWGN) and multipath slow fading channels. Based on the extrinsic information transfer (EXIT) chart technique, we investigate the convergence behavior of an iterative minimum bit error rate (MBER) multiuser detection (MUD) scheme as a function of both the system parameters and channel conditions in comparison to the SIC aided minimum mean square error (SIC-MMSE) MUD. Our simulation results show that the EXIT chart analysis is sufficiently accurate for the MBER MUD. Quantitatively, a two-antenna system was capable of supporting up to $K=6$ users at $E_b/N_0=3$dB, even when their angular separation was relatively low, potentially below $20°$.

Index Terms— Minimum bit error rate, beamforming, multiuser detection, soft interference cancellation, iterative processing, EXIT chart.

I. INTRODUCTION

THE increasing demand for mobile communication services supported within a limited radio-frequency bandwidth motivates the design of antenna array assisted beamforming techniques [1] as well as spatial division multiple access (SDMA) arrangements [2]. By appropriately combining the signals received by the different elements of an antenna array, beamforming becomes capable of creating an angularly selective transmitter/receiver beam, hence potentially separating signals transmitted on the same carrier frequency but arriving from sufficiently different angles.

Since the discovery of turbo codes [3], iterative detection [4] has been applied in the context of joint channel estimation and equalization [5], in multiuser detection [6] and numerous other coded communication systems [7]–[9]. In iterative multiuser receivers, the MUD and the channel decoder exchange extrinsic information in a number of consecutive iterations. During each iteration, the extrinsic information extracted alternately from either the MUD or the channel decoder is used as the *a priori* input by the other stage in the next iteration. The information exchanged is exploited for the sake of improving the receiver's attainable performance. In [7], a suboptimal linear MUD was introduced, which benefitted from both soft interference cancellation and instantaneous linear minimum mean squared error filtering.

Most papers discuss the minimum mean square error soft interference cancellation iterative receiver [7]–[11]. However, the MMSE algorithm does not guarantee the direct and explicit minimization of the system's BER. Hence in references [12], [13] the BER rather than the MSE was minimized at the MUD's output. The MBER beamforming design is the true optimal solution and hence it generally outperforms the MMSE solution, particularly in the context of the so-called rank-deficient systems, where the degree of freedom provided by the antenna array is lower than the number of users. The achievable BER difference of the MMSE and MBER receivers becomes particularly substantial in this scenario.

The concept of EXIT charts was introduced in [14]–[16]. This semi-analytic technique uses the mutual information between the inputs and outputs of the concatenated receiver components in order to analyze their achievable performance. For example, EXIT charts were employed in turbo equalization in [10], while in [9] and [11] they were used to examine the convergence properties of a turbo MUD. Until recently EXIT chart analysis was only capable of predicting the achievable decoding performance, when the extrinsic information was Gaussian distributed, but Li and Wang [11] succeeded in adopting this technique also in the context encountering a non-Gaussian distribution at the output of a turbo MUD.

Against this background, the novel contribution of this treatise is that iterative MBER detection is proposed for the first time in a journal paper and its performance is studied with the aid of multi-user EXIT charts. The structure of this contribution is as follows. In Section II, we outline the signal model used, followed by the portrayal of our iterative beamformer design. The focus of Section III is the novel MBER soft-input soft-output (SISO) interference canceller advocated. Section IV introduces the EXIT chart principles. Our simulation results and EXIT chart analysis are presented in Section V, followed by our conclusions in Section VI.

II. SYSTEM DESCRIPTION

A. Signal Model

The system supports K binary phase shift keying (BPSK) users and each user transmits his/her signal on the same carrier frequency of $\omega=2\pi f$. The receiver is equipped with a linear antenna array consisting of L elements, which have a uniform element spacing of $\lambda/2$, where λ is the wavelength. Assume that the channel is non-dispersive in both the angular and the time domain and hence does not induce intersymbol interference (ISI). Then the symbol-rate received signal samples can be expressed as $r_l(i)=\sum_{k=1}^{K} A_k s_k(i)e^{j\omega t_l(\theta_k)}+n_l(i)$ for $1\leq l\leq L$, where A_k

is the non-dispersive complex-valued channel coefficient of user k, $s_k(i)$ is the ith symbol of the kth BPSK user, $n_l(i)$ is a complex-valued Gaussian white noise process associated with $E[|n_l(i)|^2]=2\sigma_n^2$, and $t_l(\theta_k)=\frac{\lambda}{2}(l-1)\sin(\theta_k)/c$ is the relative time delay at array element l for the source signal of user k, with θ_k being the line of sight (LOS) angle of arrival for source k, and c is the speed of light. The received signal vector $\mathbf{r}(i)=[r_1(i)\ r_2(i)\cdots r_L(i)]^T$ is given by $\mathbf{r}(i)=\mathbf{Hs}(i)+\mathbf{n}(i)$, where we have $\mathbf{n}(i)=[n_1(i)\quad n_2(i)\cdots n_L(i)]^T$, the transmitted symbol vector of the K users is $\mathbf{s}(i)=[s_1(i)\ s_2(i)\cdots s_K(i)]^T$ and the system matrix is denoted by $\mathbf{H}=[\mathbf{h}_1\ \mathbf{h}_2\cdots\mathbf{h}_K]$, which is associated with the steering vector $\mathbf{h}_k=[A_k e^{j\omega t_1(\theta_k)}\quad A_k e^{j\omega t_2(\theta_k)}\cdots A_k e^{j\omega t_L(\theta_k)}]^T$ of source k, $k=1,\cdots,K$. The system vector $\mathbf{h}_k$ is the unique, user-specific signature of user k. In this paper, we assume that the relative time delay of all users with respect to the angularly closest neighbours is the same. All the angular locations of the users were selected under this constraint.

B. Iterative Multiuser Beamforming Receiver Structure

The iterative multiuser beamforming receiver's structure is shown in Fig. 1, which consists of two stages, namely the SISO interference cancellation aided beamforming multiuser detector, followed by K parallel single-user SISO channel decoders. The two stages are separated by the usual bit-based deinterleavers and interleavers.

The proposed SISO beamforming MUD first computes the estimated symbol $\hat{s}_k(i)$ corresponding to the transmitted symbol $s_k(i)$ using a linear filter, which determines the coefficients of the beamformer weight vector $\mathbf{w}_k(i)$ according to the specific design criterion employed and uses this weight vector to estimate $\hat{s}_k(i)$ from the received signal $\mathbf{r}(i)$ with the aid of a linear transformation [6]. Let us now define $b_k(i)$ as the only bit of the BPSK symbol $s_k(i)$, whereas $b_k(j)$ is the same bit but in a different position of the bit-based interleaving block after the deinterleaver. We will use the subscripts m and c that are associated with the multiuser detector and channel decoder, respectively, while the subscripts pr, po and e are used for representing the *a priori*, *a posteriori* and extrinsic information. Then the SISO beamforming MUD delivers the *a posteriori* information of bit $b_k(i)$ expressed in terms of its log-likelihood ratio (LLR) as [4]

$$L_{m,po,b_k(i)}=\ln\frac{\mathrm{P}[\hat{s}_k(i)|b_k(i)=0]}{\mathrm{P}[\hat{s}_k(i)|b_k(i)=1]}+\ln\frac{\mathrm{P}[b_k(i)=0]}{\mathrm{P}[b_k(i)=1]}$$
$$=L_{m,e,b_k(i)}+L_{m,pr,b_k(i)}, \qquad (1)$$

where the second term, denoted by $L_{m,pr,b_k(i)}$, represents the *a priori* LLR of the interleaved and encoded bits $b_k(i)$. The first term in Equation (1), which is denoted by $L_{m,e,b_k(i)}$, represents the extrinsic information delivered by the SISO multiuser detector, based on the received signal $\mathbf{r}(i)$ and on the *a priori* information about the encoded bits of all users, except for the bit of the desired user k. The extrinsic information is then deinterleaved and fed into the kth user's channel decoder, which will provide the *a priori* information in the next iteration.

As seen in Fig. 1, between the banks of channel decoders and interleavers, we compute the extrinsic LLR

based on the *a priori* information $L_{c,pr,b_k}(j)$ provided by the SISO beamforming MUD for the SISO decoder as $L_{c,e,b_k}(j)=L_{c,po,b_k}(j)-L_{c,pr,b_k}(j)$ [4], where the extrinsic information is gleaned from the surrounding encoded bits, excluding the specific bit considered [5]. After interleaving, the extrinsic information delivered by the channel decoders is then fed back to the SISO multiuser detector, as the *a priori* information concerning the encoded bits of all the users for exploitation during the next iteration.

III. SISO INTERFERENCE CANCELLATION

As described in the previous section, the task of SISO interference cancellation is to choose the beamformer weight vector $\mathbf{w}_k$ of the linear filter seen in Fig. 1 according to an appropriate design criterion and compute the corresponding output LLRs.

Given the *a priori* LLRs, we first define the mean and variance of the kth user's symbols for BPSK as [8] where the symbol-index i was dropped for notational convenience:

$$\bar{s}_k=\mathrm{E}[s_k]=\tanh(\frac{L_{pr,b_k}}{2}), \qquad (2)$$

and

$$v_k=\mathrm{Cov}[s_k,s_k]=1-\tanh^2(\frac{L_{pr,b_k}}{2}). \qquad (3)$$

When using the soft interference cancellation principle, the estimated symbol of user k can be expressed as [8]

$$\hat{s}_k=\mathbf{w}_k^H(\mathbf{r}-\mathbf{H}\bar{\mathbf{s}}+\mathbf{h}_k\bar{s}_k), \qquad (4)$$

where we have $\bar{\mathbf{s}}=[\bar{s}_1\ \bar{s}_2\cdots\bar{s}_K]^T$. In the next three sections we will outline the differences of the real-valued as well as complex-valued MMSE MUD and contrast them to the MBER MUD.

A. SISO Interference Cancellation Using the Complex-Valued MMSE MUD

Classically, the complex-valued MMSE (CMMSE) solution of the beamformer's weight vector $\mathbf{w}_k$ is expressed as [8]

$$\mathbf{w}_{k,cmmse}=(\mathbf{HVH}^H+|\bar{s}_k|^2\mathbf{h}_k\mathbf{h}_k^H+2\sigma_n^2\mathbf{I}_L)^{-1}\mathbf{h}_k, \quad (5)$$

where $\mathbf{I}_L$ denotes the $(L\times L)$-dimensional identity matrix and we have $\mathbf{V}=\mathrm{diag}[v_1\ v_2\cdots v_K]$.

As stated in [8], the conditional probability density function (PDF) $\mathrm{P}[\hat{s}_k|s_k=s_k^{(q)}]$, where $s_k^{(q)}$ is the qth ($q=1,2$) legitimate value of the symbol s_k, may be assumed to be Gaussian distributed and the extrinsic output LLR is given by

$$L_{e,b_k}=\frac{4\Re[\mathbf{w}_k^H(\mathbf{r}-\mathbf{H}\bar{\mathbf{s}}+\bar{s}_k\mathbf{h}_k)]}{1-v_k\mathbf{w}_k^H\mathbf{h}_k} \qquad (6)$$

for BPSK, where $\Re[\cdot]$ denotes the real part.

B. SISO Interference Cancellation Using the Real-Valued MMSE MUD

For BPSK systems, the beamformer's desired output s_k is real-valued. It is clear that the CMMSE solution of Section III-A attempts to simultaneously minimize the MSE between the desired signal and both the real part and imaginary part of the beamformer's output. However, in case of BPSK modulation
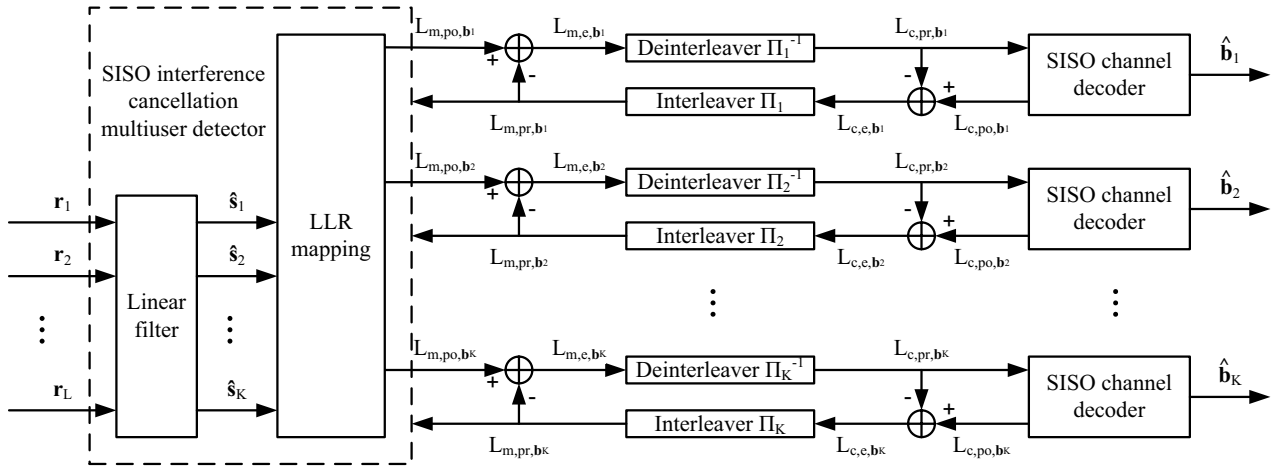
Fig. 1.   Iterative multiuser beamforming receiver structure

the beamformer's decision depends only on the real part of the multiuser signal at the beamformer's output. Hence minimizing the MSE associated with the imaginary part does not contribute to improving the beamformer's performance. Quite the opposite, it rather imposes an unnecessary constraint on the beamforming weights [17]. Hence we introduce the real-valued MMSE (RMMSE) solution.

The real-valued MSE cost function minimizing the MSE between the desired signal and the real part of the beamformer's output can be written as

$$J_{rmse}(\mathbf{w}_k) = \mathrm{E}[(s_k - \hat{s}_{k,R})^2], \tag{7}$$

where we have $\hat{s}_{k,R} = \Re[\hat{s}_k]$. The RMMSE solution is defined by $\mathbf{w}_{k,rmmse} = \arg\min_{\mathbf{w}} J_{rmse}(\mathbf{w}_k)$. The gradient of $J_{rmse}(\mathbf{w}_k)$ is given by

$$\nabla J_{rmse}(\mathbf{w}_k) = (\mathbf{HVH}^H + \bar{s}_k^2 \mathbf{h}_k \mathbf{h}_k^H + 2\sigma_n^2 \mathbf{I}_L)\mathbf{w}_k + (\mathbf{HVH}^T + \bar{s}_k^2 \mathbf{h}_k \mathbf{h}_k^H)\mathbf{w}_k^* - 2\mathbf{h}_k. \tag{8}$$

In order to derive a closed-form solution for this RMMSE design, we apply the real-valued vertical concatenation matrix method of [17]. Let us define the index c as the subscript to indicate the matrices' vertical concatenation, then we have $\mathbf{M}_c = (\Re[\mathbf{M}]^T \, \Im[\mathbf{M}]^T)^T$, where $\mathbf{M}_c$ can be any matrix which is vertically concatenated. Hence, the gradient of Equation (7) becomes

$$\nabla J_{rmse}(\mathbf{w}_{k,c}) = 2(\mathbf{H}_c \mathbf{V} \mathbf{H}_c^T + \bar{s}_k^2 \mathbf{h}_{k,c} \mathbf{h}_{k,c}^T + \sigma_n^2 \mathbf{I}_{2L})\mathbf{w}_{k,c} - 2\mathbf{h}_{k,c}. \tag{9}$$

Then, in contrast to the closed-form CMMSE solution of Equation (5), the closed-form solution of the concatenated weight matrix $\mathbf{w}_{k,rmmse,c}$ is derived from Equation (9), yielding

$$\mathbf{w}_{k,rmmse,c} = (\mathbf{H}_c \mathbf{V} \mathbf{H}_c^T + \bar{s}_k^2 \mathbf{h}_{k,c} \mathbf{h}_{k,c}^T + \sigma_n^2 \mathbf{I}_{2L})^{-1} \mathbf{h}_{k,c}. \tag{10}$$

The first L elements of $\mathbf{w}_{k,rmmse,c}$ are the real part of the RMMSE solution $\mathbf{w}_{k,rmmse}$, and the last L elements of $\mathbf{w}_{k,rmmse,c}$ form the imaginary part of $\mathbf{w}_{k,rmmse}$.

The conditional PDF $\mathrm{P}(\hat{s}_k | s_k = s_k^{(q)})$ is a mixture of all legitimate transmitted signals' distributions, when the kth user transmits symbol $s_k^{(q)}$ and all other interfering users transmit

an arbitrary symbol. Unlike in case of the CMMSE solution, this conditional PDF cannot be assumed to be Gaussian distributed in the RMMSE design. The MSE minimization of the RMMSE solution considers only the inphase component and we assume that the real part of the PDF is Gaussian [18]. The conditional mean and variance of $\hat{s}_{k,R}$ are given by

$$\mu_{k,R}^{(q)} = \mathrm{E}[\hat{s}_{k,R} | s_k = s_k^{(q)}] = s_k^{(q)} \mathbf{w}_{k,c}^T \mathbf{h}_{k,c} \tag{11}$$

and

$$\sigma_{k,R}^2 = \mathrm{Cov}[\hat{s}_{k,R}, \hat{s}_{k,R} | s_k = s_k^{(q)}] = \mathbf{w}_{k,c}^T \mathbf{h}_{k,c}(1 - \mathbf{w}_{k,c}^T \mathbf{h}_{k,c}). \tag{12}$$

Given

$$\mathrm{P}(\hat{s}_{k,R} | \mathbf{r}, s_k = s_k^{(q)}) = \frac{1}{\sqrt{2\pi}\sigma_{k,R}} \exp\left(-\frac{(\hat{s}_{k,R} - \mu_{k,R}^{(q)})^2}{2\sigma_{k,R}^2}\right), \tag{13}$$

the extrinsic output LLR can be expressed as

$$L_{e,b_k} = \frac{2\mathbf{w}_{k,c}^T(\mathbf{r}_c - \mathbf{H}_c \bar{\mathbf{s}} + \bar{s}_k \mathbf{h}_{k,c})}{1 - \mathbf{w}_{k,c}^T \mathbf{h}_{k,c}}. \tag{14}$$

C. SISO Interference Cancellation Using the MBER MUD

In BPSK systems supporting K users, the transmitted K-user symbol combination may assume $N_b = 2^K$ possible combinations. By defining $x_{k,R} = \mathrm{sgn}(s_{k,R}) \cdot \hat{s}_{k,R}$, the conditional PDF of $x_{k,R}$ is a Gaussian mixture[1] given by [12]

$$\mathrm{P}(x_{k,R}; \mathbf{w}_k) = \frac{1}{\sqrt{2\pi}\sigma_n \sqrt{\mathbf{w}_k^H \mathbf{w}_k}} \sum_{q=1}^{N_b} \mathrm{P}(\mathbf{s}^{(q)})$$
$$\cdot \exp\left(-\frac{(x_{k,R} - \mathrm{sgn}(s_{k,R}^{(q)}) \cdot \bar{\hat{s}}_{k,R}^{(q)})^2}{2\sigma_n^2 \mathbf{w}_k^H \mathbf{w}_k}\right) \tag{15}$$

where $\mathrm{P}(\mathbf{s}^{(q)}) = \prod_k \mathrm{P}(s_k = s_k^{(q)})$ is the *a priori* probability of transmitting the qth ($q = 1, 2, \cdots, 2^K$) possible symbol combination $\mathbf{s}^{(q)}$ of the K users, and $\bar{\hat{s}}_{k,R}^{(q)}$ is the real part of the kth

---

[1]A Gaussian mixture is constituted by the weighted sum of Gaussian densities, where the weights are all positive and sum to unity.

user's estimated symbol. When ignoring the effects of noise, we have

$$\bar{s}_{k,R}^{(q)} = \Re[\mathbf{w}_k^H(\mathbf{H}\mathbf{s}^{(q)} - \mathbf{H}\bar{\mathbf{s}} + \bar{s}_k\mathbf{h}_k)]. \tag{16}$$

It can be readily shown that the error probability of the real part is [12]

$$\begin{aligned}
\mathrm{Pe}_{k,R}(\mathbf{w}_k) &= \mathrm{P}(x_{k,R}{<}0) \\
&= \sum_{q=1}^{N_b} \mathrm{P}(\mathbf{s}^{(q)}) \cdot Q\left[\frac{\mathrm{sgn}(s_{k,R}^{(q)}) \cdot \bar{s}_{k,R}^{(q)}}{\sigma_n\sqrt{\mathbf{w}_k^H\mathbf{w}_k}}\right], \quad (17)
\end{aligned}$$

where $Q[x]{=}(1/\sqrt{2\pi})\int_{-\infty}^{x} e^{-t^2/2}dt$. The MBER beamforming solution for BPSK is then defined as [12]

$$\mathbf{w}_{k,mber} = \arg\min_{\mathbf{w}} \mathrm{Pe}_{k,R}(\mathbf{w}_k). \tag{18}$$

This optimization problem can be solved using the simplified conjugate gradient algorithm, which is detailed in [12]. The gradient of the bit error probability is given by

$$\begin{aligned}
\nabla\mathrm{Pe}_{k,R}(\bar{\mathbf{w}}_k) &= \frac{1}{\sqrt{2\pi}\sigma_n} \sum_{q=1}^{N_b} \mathrm{P}(\mathbf{s}^{(q)}) \exp\left(-\frac{(\bar{s}_{k,R}^{(q)})^2}{2\sigma_n^2}\right) \\
&\quad \cdot \mathrm{sgn}(s_{k,R}^{(q)}) \cdot (\bar{\mathbf{w}}_k\bar{s}_{k,R}^{(q)} - (\mathbf{H}\mathbf{s}^{(q)} - \mathbf{H}\bar{\mathbf{s}} + \bar{s}_k\mathbf{h}_k)),
\end{aligned} \tag{19}$$

where $\bar{\mathbf{w}}_k$ is the unity-norm normalized version of the vector $\mathbf{w}_k$.

In the MBER design, the real part of the estimated symbols are non-Gaussian. Hence the challenge is that we cannot use the Gaussian approximation for calculating the output extrinsic LLRs of the MBER multiuser detector. The exact expression of the extrinsic information delivered by the MUD is [6]

$$L_{e,b_k} = \ln\frac{\sum_{\forall\mathbf{s}^{(q)}:b_k^{(q)}=0} \mathrm{P}(\hat{s}_k|\mathbf{s}^{(q)})\prod_{\forall k':k'\neq k}\mathrm{P}(b_{k'}^{(q)})}{\sum_{\forall\mathbf{s}^{(q)}:b_k^{(q)}=1} \mathrm{P}(\hat{s}_k|\mathbf{s}^{(q)})\prod_{\forall k':k'\neq k}\mathrm{P}(b_{k'}^{(q)})}, \tag{20}$$

where we have

$$\mathrm{P}(\hat{s}_k|\mathbf{s}^{(q)}) = \frac{1}{\sqrt{2\pi}\sigma_n} \exp\left(-\frac{\Re^2[\bar{\mathbf{w}}_k^H(\mathbf{r} - \mathbf{H}\mathbf{s}^{(q)})]}{2\sigma_n^2}\right), \tag{21}$$

which represents the conditional probability of the real part of the kth user's estimated symbol, when transmitting the qth combination $\mathbf{s}^{(q)}$. Furthermore [3],

$$\mathrm{P}(b_{k'}^{(q)}) = \frac{1 + \mathrm{sgn}(b_{k'}^{(q)})\tanh(\frac{L_{pr,b_{k'}}}{2})}{2} \tag{22}$$

is the probability of the k'th user's bit in case of the qth K-user symbol combination using the *a priori* information.

Table I shows the computational complexity comparison of the weight calculations and the output extrinsic LLR calculations for the above-mentioned three different MUD algorithms. The symbol N_{cg} indicates the number of iterations required by the simplified conjugate gradient algorithm for obtaining the MBER MUD's weights. The computational complexity of CMMSE and RMMSE MUD algorithms is similar, both of which are proportional to L^3 due to the required matrix inversion operations. The MBER MUD solution is more complex, and its complexity is proportional to $N_{cg}2^K$.

TABLE I
COMPARISON OF COMPUTATIONAL COMPLEXITY FOR THE CMMSE, RMMSE AND MBER MUDs

MUD algorithm		Computational complexity
CMMSE	Weight	$4KL^2+2KL+10L^2$ real-valued multiplications, $4KL^2+6L^2-L$ real-valued additions, and 1 complex-valued ($L\times L$) matrix inverse
	LLR	$2KL+6L+3$ real-valued multiplications, and $2KL+6L-1$ real-valued additions
RMMSE	Weight	$4KL^2+2KL+12L^2$ real-valued multiplications, $4KL^2+4L^2$ real-valued additions, and 1 real-valued ($2L\times2L$) matrix inverse
	LLR	$2KL+6L+2$ real-valued multiplications, and $2KL+6L-1$ real-valued additions
MBER	Weight	$N_{cg}[(3L+4)2^K+4KL+13L+3]$ $+(4KL+4L)2^K$ real-valued multiplications, $N_{cg}(3L2^K+4KL-2K+7L-2)$ $+(2KL+4K+4L-2)2^K$ real-valued additions, and $N_{cg}2^K$ exponent operations
	LLR	$(4KL+K+2L+5)2^K+1$ real-valued multiplications, $(3KL+2L+1)2^K-2$ real-valued additions, and 2^K+1 exponent operations

IV. EXIT CHART ANALYSIS FOR MULTIUSER BEAMFORMING

For the sake of EXIT chart analysis, the receiver components (i.e., the multiuser detector and the channel decoder) are modeled as components mapping a sequence of received signal observations and the *a priori* information L_i to a new sequence constituting the extrinsic information L_o. The EXIT chart analysis computes the mutual information between the LLRs L_i and the corresponding bits S, as given in [14]. After passing samples of L_i through the detector or the decoder, at the output the mutual information $I(L_o; S)$ between the extrinsic information L_o and S is obtained by using the distribution of L_o. This can be done by first approximating the PDF of L_o by the experimentally generated histogram of the output LLRs and then computing $I(L_o; S)$ numerically. We denote the mutual information of the input and output LLRs, respectively by $I_i{=}I(L_i; S)$ and $I_o{=}I(L_o; S)$.

Note that for the MUD, the received signal has to be recorded for a given channel state and signal-noise-ratio (SNR), because the MUD's received signal is affected by the channel quality quantified here in terms of the noise power. The EXIT chart is either the nonlinear transfer function $I_{m,o}{=}f_m(I_{m,i}, SNR)$ of the MUD or the corresponding function $I_{c,o}{=}f_c(I_{c,i})$ of the channel decoder, which maps the input variable I_i to the output variable I_o. The specific value of I_o in the range $[0, 1]$ characterizes the quality of the output LLRs of a receiver component. We generate the EXIT curve $I_o{=}f(I_i)$ by assuming the *a priori* LLRs are Gaussian distributed. This simplifying assumption results in a discrepancy between the EXIT charts and the actually encountered real detection or decoding trajectories. This discrepancy is maybe sufficiently low so that we may ignore it [19]. When using the mutual information as our detection convergence metric, we do not require that the distribution of the output extrinsic information has to be Gaussian, since the mutual information is a function of the entire PDF, rather than that of the first and second moments of the extrinsic information. Based on this feature, EXIT chart analysis can also be applied to multiuser communications over multipath fading channels, despite the

fact that in this case the distribution of the output extrinsic information of the MUD cannot be accurately approximated by a Gaussian PDF.

The output of one of the constituent detectors is the input of the other, hence both transfer functions are shown in the same EXIT plane having coordinate axes of $(I_{m,i}=I_{c,o}), (I_{m,o}=I_{c,i})$. The stair-case-shaped lines connecting the mutual information points evaluated during each iteration are referred to as the detection or decoding trajectory. The substantial advantage of EXIT charts accrues from the fact that the detection trajectory points recorded for both constituent components exchanging information fall on the continuous EXIT functions obtained independently in a separate process. An infinitesimally low BER may be attained, when there is a so-called open tunnel between the EXIT curves of the decoder and the MUD, as seen in Fig. 2 for $E_b/N_0=$4dB. This graphical representation gives us an immediate insight into the number of detection iterations required to attain the best possible BER performance. Finally, since the mutual information at the decoder's output may be directly mapped to the final BER [11], EXIT charts allow us to compare turbo receivers in terms of their overall BER performance.

Unlike in single-user turbo coding or turbo equalization, in the multiuser detection scenario the MUD's EXIT curve recorded for the desired user depends on all the other $(K-1)$ users' channel decoder output mutual information, which implies that the MUD's EXIT surface should be K-dimensional. Unfortunately this K-dimensional EXIT hyperplane cannot be readily visualized. A feasible solution to resolve this problem is that of translating a single K-dimensional EXIT chart to K number of two-dimensional EXIT charts, where each two-dimensional EXIT chart corresponds to a single user. However, the MUD's EXIT curve in any of these two-dimensional EXIT charts changes upon each iteration, and it also depends on the other users' mutual information forwarded from the channel decoders to the MUD. Nonetheless, we now slightly relaxed our simplifications and we assume that although all the users' angular locations are selected so that the relative time delay of all users with respect to the angularly closest neighbors is the same, one of the users has a higher power than the remaining equal-power users. In CDMA or SDMA systems, if all the cross-correlation coefficients are equal, the multiuser interference (MUI) imposed by any of the users is equivalent. Hence we can use a pair of 2D EXIT charts for analyzing the attainable convergence performance. More specifically, one of the EXIT charts is for the higher-power user, where the EXIT curves do not depend on the iteration index, while the other EXIT chart is for the average of the lower-power users, where the MUD's EXIT curve depends on the iteration index. However, in the context of beamforming systems operating under the above-mentioned conditions, the high-power user always imposes more interference on the angularly adjacent users than on the angularly better separated users. This implies that during the first iteration, the low-power users who are angularly close to the high-power user have a worse performance than the other low-power users. Furthermore, during later iterations, when a high-power user has a lower BER and can be essentially canceled, the angularly adjacent low-power users will have a better performance than the others. Hence

TABLE II
SYSTEM PARAMETERS

Number of receive antennas	2
Number of users	$1, 3, 4, 5, 6, 7, 8$
Arrival angles of users' signal	Single user: $15°$
	3 users: $15°, -24°, 68°$
	4 users: $15°, -48°, -14°, 49°$
	5 users: $15°, -8°, 41°, -33°, -70°$
	6 users: $15°, -24°, 68°, -4°, 36°,$ $-48°$
	7 users: $15°, -2°, 33°, -18°, 56°,$ $-37°, -62°$
	8 users: $15°, -48°, -14°, 49°, 31°,$ $1°, -82°, -29°$
Modulation	BPSK
Interleaving length	2×10^4
MUD	CMMSE, RMMSE, MBER
Channel coding	NSC, RSC
Code rate	$1/2$
Constraint length	4
Polynomial generators	NSC: $(15, 17)$
	RSC: $(13, 6)$
Channels	AWGN, multipath fading
The following parameters are only for multipath fading channel scenarios	
Number of multipath	3
Multipath power	$0, -5, -10$dB
Multipath delay	$0, 25T_s, 50T_s$
Number of OFDM subcarriers	512
OFDM cyclic prefix length	64

the low-power users' signals cannot be readily combined into a single subset and hence their performance cannot be directly averaged. Therefore the 2D EXIT charts are unsuitable even for this simple beamforming scenario. Based on the above reasons, in our simulations all users' SNRs were identical. Additionally, their angular locations were selected so that the relative time delay of all users with respect to the angularly closest neighbors was the same, as defined in Section II-A. Hence the turbo MUD can average all the users' mutual information in order to generate the corresponding EXIT chart. When these constraints are not satisfied, the averaged EXIT trajectories will deviate from the EXIT transfer curves and consequently the EXIT chart analysis becomes less accurate.

V. SIMULATION RESULTS

In this section, we use EXIT charts to analyze the attainable performance of the iterative MBER beamforming receiver. The system employs a two-element antenna array. All users employ BPSK modulation and have the same transmit power as well as channel coefficients of $A_k=1.0 + j0.0$ (for $1 \leq k \leq K$), except for Section V-G, where the system communicates over multipath slow-fading channels. The system parameters and the angular separation of users with respect to the antenna array are shown in Table II. Each user employs a different randomly generated interleaver. The interleaver length of each user is 2×10^4 bits.

A. EXIT-Chart Trajectories of the MBER MUD

According to the principles outlined in Section IV, in Fig. 2 we plot both the EXIT charts and the simulated trajectories of the iterative MBER beamforming receiver supporting $K=6$ users at $E_b/N_0=$2dB, 3dB and 4dB. All users employ the
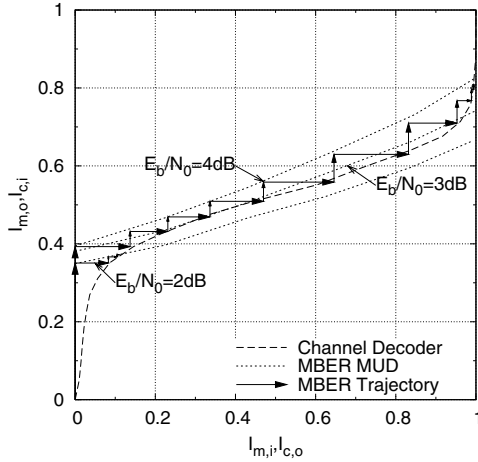
Fig. 2. EXIT charts and simulated trajectories of the iterative MBER receiver supporting $K=6$ users at $E_b/N_0=$2dB, 3dB and 4dB

TABLE III
COMPARISON OF BER ESTIMATION FROM EXIT CHART AND SIMULATION RESULTS

Iteration index	$I_{c,i}, I_{c,o}$	$\sigma_{c,i}, \sigma_{c,o}$	Estimated BER	Simulated BER
0	0.393, 0.137	1.72, 0.915	1.647e-1	2.497e-1
1	0.432, 0.231	1.84, 1.23	1.346e-1	1.928e-1
2	0.469, 0.336	1.95, 1.55	1.066e-1	1.468e-1
3	0.509, 0.47	2.07, 1.95	7.78e-2	1.013e-1
4	0.558, 0.646	2.23, 2.53	4.599e-2	5.672e-2
5	0.63, 0.832	2.47, 3.38	1.808e-2	2.099e-2
6	0.71, 0.953	2.78, 4.51	4.025e-3	5.117e-3
7	0.767, 0.989	3.03, 5.55	7.888e-4	1.198e-3
8	0.796, 0.994	3.18, 5.96	3.624e-4	6.1e-4
9	0.804, 0.995	3.22, 6.04	3.131e-4	4.133e-4
10	0.808, 0.996	3.24, 6.24	2.199e-4	3.883e-4

same rate $1/2$ and constraint length 4 NSC code using the octally represented generators $(15, 17)$.

The iterative detection process commences from the $I_{m,i}=0$ point, which implies the absence of *a priori* information for the MUD. Next, the output LLRs described by $I_{m,o}=I_{c,i}$ are fed into the decoder, yielding the LLRs described by $I_{c,o}=I_{m,i}$, which are then fed back to the MUD and so forth. The detection process is curtailed at the crossing of the EXIT curves of the MUD and the decoder if the SNR is insufficiently high, as seen for $E_b/N_0=$2dB in Fig. 2. The iterative detection process is represented by the staircase shaped trace between the transfer curves of the MUD (the doted line) and decoder (the dashed line) components.

Fig. 2 also shows the detection trajectories (the solid lines with arrows) of the iterative process obtained by simulation. The detection trajectories closely follow the EXIT curves of the receiver components, which indicates that the EXIT chart analysis is valid for the MBER MUD. Again, as seen in Fig. 2, at $E_b/N_0=$2dB the trajectory is curtailed after two iterations, since the EXIT curves of the MUD and the decoder do intersect. By contrast, at $E_b/N_0=$4dB, the decoding trajectory passes through "the bottleneck" and reaches the top-right corner, indicating an infinitesimally low BER. We observe that after a few iterations, the trajectories slightly deviate from the EXIT curves, which is a consequence of the extrinsic information becoming correlated upon increasing the number of iterations, in particular, when the interleaving length is finite.

B. EXIT-Chart Based BER Estimation

EXIT charts can be used to obtain an estimate of the BER after an arbitrary number of iterations. For the channel decoder, the soft output of the coded bits generated after a given number of iterations can be written as the sum of the extrinsic information and the *a priori* information, which can be expressed as $L=L_{c,i} + L_{c,o}$. For the sake of deriving a simple formula for the channel coded bit error probability P_b, both the *a priori* information $L_{c,i}$ and the extrinsic information $L_{c,o}$ are assumed to be Gaussian distributed. Hence, the decoder's output L is also Gaussian with a variance of σ^2

and a mean of $\mu=\sigma^2/2$. Then the coded bit error probability can be written as [15]

$$P_b \approx Q\left[\frac{\sigma}{2}\right]. \qquad (23)$$

Assuming perfect independence between the extrinsic information and the *a priori* information, we have $\sigma^2=\sigma_{c,i}^2 + \sigma_{c,o}^2$. The variances $\sigma_{c,i}^2$ and $\sigma_{c,o}^2$ can be obtained from the corresponding mutual information $I_{c,i}$ and $I_{c,o}$, since the functions are monotonically increasing and hence they are invertible [15].

Consider a six-user system communicating over an AWGN channel. We use a rate $1/2$ NSC code having the octal generators of $(15, 17)$. Table III compares the estimated coded BER results obtained from the EXIT chart to the simulation results characterizing the iterative MBER MUD at $E_b/N_0=$4dB. The table shows that the EXIT chart in combination with the Gaussian approximation provides reasonable BER predictions.

C. Operating SNR Threshold Estimation

We can infer from the above results that the turbo detection scheme is capable of providing significant performance improvements, when the iterative process converges successfully. However, achieving successful convergence depends upon a number of factors, such as the user load, the type of detector, as well as the channel code and the SNR considered, all of which will be considered below.

From Fig.2, it is readily seen that if E_b/N_0 is higher than 3.0dB, there is an open tunnel between the EXIT curve of the MUD and that of the decoder. The iterative process will hence successfully converge to an infinitesimally low BER. However, if E_b/N_0 is lower than 3.0dB, the EXIT tunnel will close and the iterative process fails to provide a significant BER performance improvement. Hence we refer to $E_b/N_0=$3.0dB as the operating SNR threshold of this system.

Fig. 3 shows the BER performance of the system, when increasing the number of iterations. It can be seen that when the SNR is higher than 3.0dB, the achievable BER approaches that of the single-user bound, which confirms the predictions of the EXIT charts. Finally, it is worth noting that the narrower the EXIT tunnel, the higher the number of iterations required for achieving detection convergence.
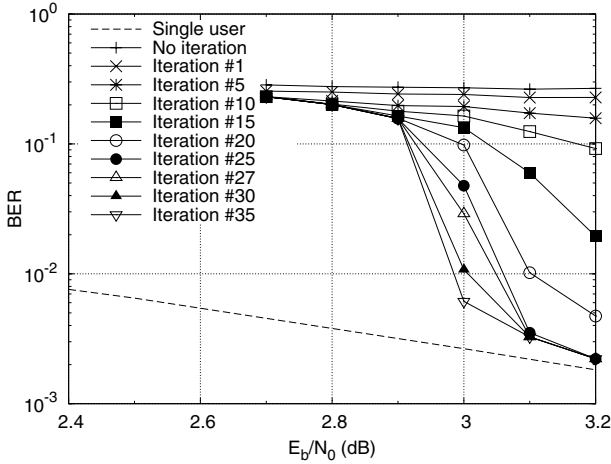
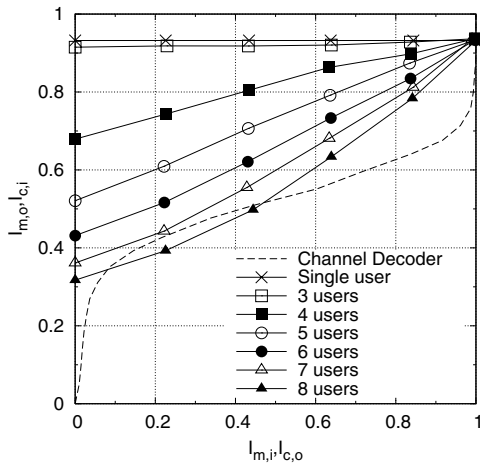Fig. 3. BER performance of the iterative MBER beamforming receiver supporting $K=6$ users

Fig. 5. EXIT characteristics of the different SISO MUDs supporting $K=6$ users at $E_b/N_0=0$dB, 3dB and 6dB

Fig. 4. EXIT charts for the MBER MUD and NSC channel decoder for different number of users at $E_b/N_0=6$dB

D. The Number of User Supported

In addition to the operating SNR threshold, there are other thresholds in turbo multiuser detection, which are of interest. For example, given a certain SNR, the EXIT curve of the detector moves downwards upon increasing the number of users K, potentially closing the convergence tunnel. This limits the maximum number of users that the system can support at this SNR.

Fig. 4 shows the EXIT curves of the channel decoder and the MBER MUD, when supporting different number of users K at $E_b/N_0=6$dB. The channel code is a rate $1/2$ NSC code having the octally represented generators of $(15, 17)$. The EXIT chart shows that at $E_b/N_0=6$dB, the maximum number of users is $K=7$, where an open EXIT-tunnel is visible. It is clear that the maximum number of users supported is a function of the SNR, as well as of the specific detection and decoding schemes employed.

Fig. 4 also shows that all the MUD EXIT curves converge to the ordinate value of $I_{m,o}\approx0.93$ at the abscissa of $I_{m,i}=1$. This is because regardless of the number of users, when the *a priori* information is perfect, all the other users' interference can be perfectly removed, resulting in a near-single-user per-
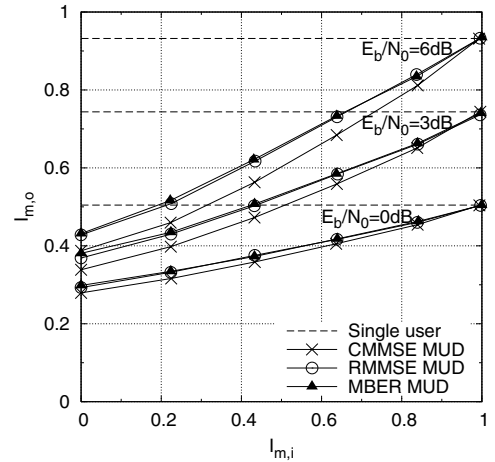
formance. We also note that the point of perfect convergence at $(1, 1)$ is not reached, since the BER performance of the MUD depends on the SNR, when the MUI has been perfectly removed. When the SNR is infinitely high, the point of $(1, 1)$ can indeed be reached.

E. Comparison of Different Turbo-MUDs

Consider a six-user system employing two receive antennas. Fig. 5 shows the EXIT characteristics of the iterative MUDs using the MBER, the complex-MMSE and the real-MMSE detection schemes operating at $E_b/N_0=0$dB, 3dB and 6dB. The MBER MUD has the potential of providing a marginally wider EXIT tunnel than the RMMSE scheme, followed by the CMMSE MUD. Fig. 5 also reveals that the three detectors yield the same value of $I_{m,o}<1$ with the advent of perfect *a priori* information corresponding to $I_{m,i}=1$. This is because for $|L_m|\rightarrow\infty$, the multiple access interference (MAI) can be completely removed from the received signal.

The main difference between the three detectors is the slope of the EXIT curves, which will then affect both the SNR convergence threshold and the convergence rate of the associated turbo receiver. Fig. 6 shows the BER versus SNR performance of these three MUD algorithms, which have minimum operating SNRs of 3.0dB, 3.2dB and 4.8dB, respectively. It can be seen that the performance of all three beamforming receivers has significantly improved after $i=35$ iterations and $i=28$ iterations, respectively. In this rank-deficient system supporting three times the number of users in comparison to the number of antennas, the MBER algorithm has the lowest operating SNR requirement.

Fig. 7 shows the lowest number of iterations required to achieve a near-single-user performance for the three MUDs, when the SNR experienced is higher than the SNR threshold. It is clear that the number of iterations required decreases upon increasing the SNR. At a given SNR, the MBER algorithm necessitates the lowest number of iterations for approaching the single-user performance. Fig. 7 also shows the number of users supported at different SNRs for the three MUDs. The MBER algorithm is likely to support more users than the other two algorithms.
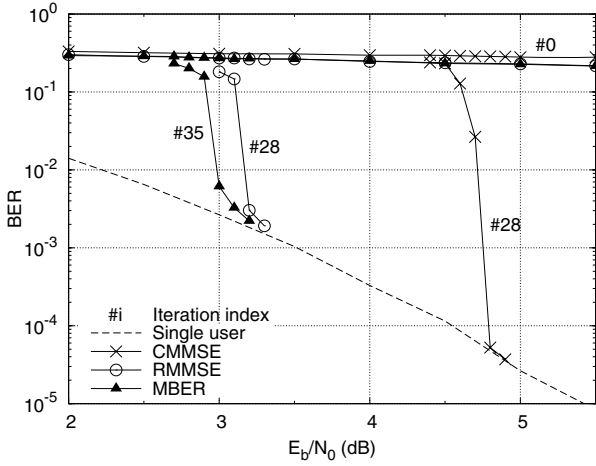
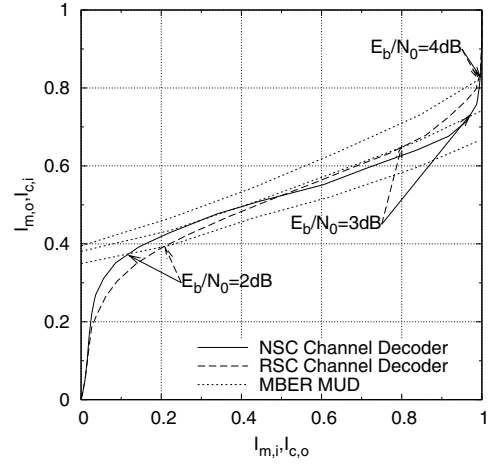Fig. 6. BER comparison of the CMMSE, RMMSE and MBER iterative MUDs supporting $K=6$ users
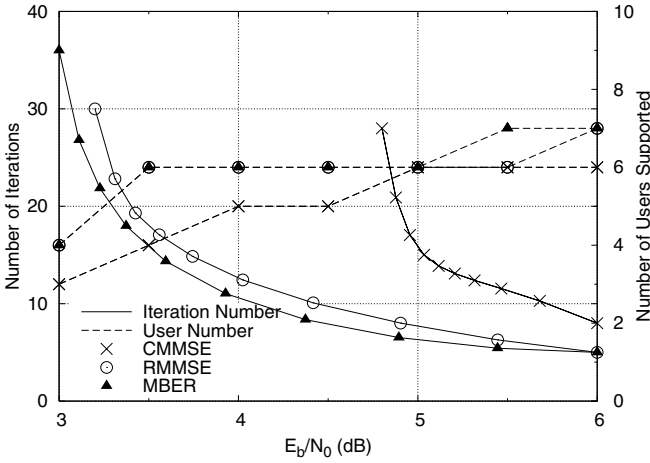

Fig. 7. The number of iterations required to achieve a near-single-user performance supporting $K=6$ users (left axis), and the number of users supported (right axis) by the different SISO MUDs

Fig. 8. EXIT charts of the NSC and RSC channel decoders along with the MBER MUD's EXIT characteristics, when supporting $K=6$ users at $E_b/N_0=2$dB, 3dB and 4dB
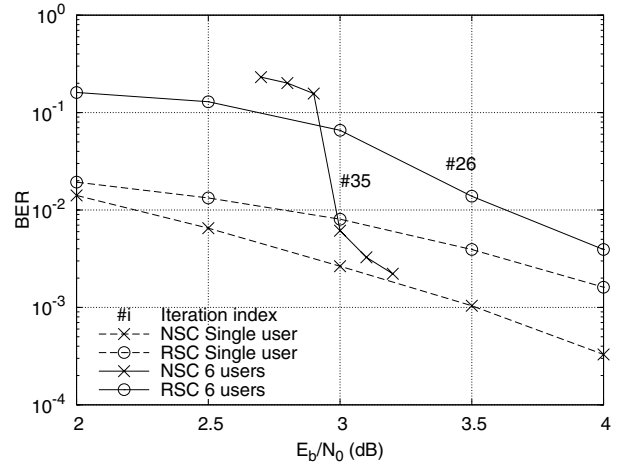

Fig. 9. BER comparison of the NSC and RSC coded MBER turbo receivers supporting $K=6$ users after $i=35$ iterations and $i=26$ iterations, respectively

F. Comparison of Different Channel Coding Schemes

Let us now compare the performance of the MBER turbo receivers using different channel codes, namely the previously used NSC code and a recursive systematic convolutional (RSC) code. Both codes have the same code rate of $1/2$ and constraint length 4. The generator polynomials are $(15, 17)$ and $(13, 6)$ in octal representation, respectively.

Fig. 8 shows the EXIT charts of the NSC and RSC channel decoders along with the MBER MUD characteristics, when supporting $K=6$ users at $E_b/N_0=2$dB, 3dB and 4dB. Observe in Fig. 8 that when $I_{c,i}$ is lower than 0.5, the RNC code has a higher output mutual information $I_{c,o}$ than the NSC code. However, as $I_{c,i}$ increases, the NSC code starts to perform better. In Fig. 8, the arrows indicate the intercept points of the channel decoders and the MBER MUD at different SNRs. When the SNR is low, for example 2dB, the intercept points of both decoders are near the bottom-left corner, with that of the NSC being nearer. This implies that the receiver using the RSC code has a better performance at low SNRs. When the SNR increases to 3dB, the NSC code provides an open EXIT tunnel and the intercept point of the NSC decoder is moved

nearer to the top-right corner than that of the RSC scheme. Hence the NSC receiver performs better. Fig. 9 shows the simulated BER performance of the NSC and RCS receivers after $i=35$ iterations and $i=26$ iterations, respectively, which confirms the above EXIT-chart based conclusions. Intuitively, this may be expected, since in general NSC codes have a better weight-distribution than their RSC counterparts.

Observe from Fig. 9 that the NSC-coded receiver has a steep BER curve, while the RSC receiver's BER curve is quite gently sloping. The reason for this difference can be explained by their EXIT charts. Comparing the EXIT characteristics of the NSC decoder and the MBER MUD at 3dB in Fig. 8, we also observe that the EXIT chart slope of the MUD is slightly steeper than that of the NSC decoder. This implies that the bottleneck is at the left end of the tunnel. When the EXIT tunnel becomes just opened, the receiver becomes capable of achieving a significant BER versus SNR gain, which results in a steep BER curve. By contrast, for the RSC code the slope of the decoder's EXIT curve is steeper than that of the MUD and hence the EXIT-chart intercept point moves more gradually upon increasing the SNR. Hence the BER curve of the RSC
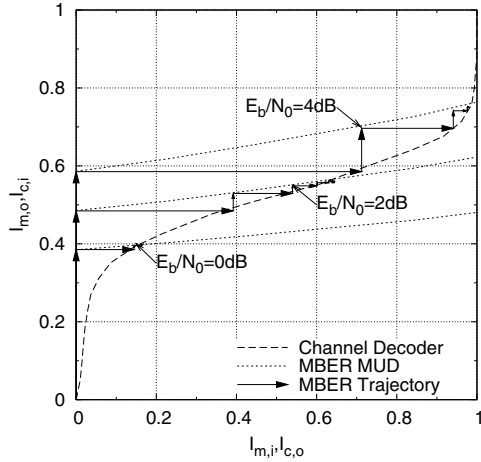
Fig. 10. EXIT charts and simulated trajectories of the iterative MBER receiver supporting $K=4$ users in multipath fading channel at $E_b/N_0=0$dB, 2dB and 4dB

Fig. 11. BER performance of the iterative MBER, CMMSE and RMMSE beamforming receiver supporting $K=4$ users in multipath fading channel

receiver does not exhibit the same waterfall phenomenon. Actually, at the threshold SNR value, the area between the two component curves is a measure of the performance loss relative to the channel capacity [16]. Therefore, both above-mentioned channel codes are somewhat deficient. To optimize the performance, we have to find a specific channel code, whose EXIT curve matches the MUD's curve in order to minimize the area between them. This will be investigated in our future work.

G. EXIT Charts of the MBER MUD in Wideband Multipath Slow-Fading Channels

Consider a $K=4$ user system communicating over wideband frequency-selective slow-fading channels. Each user's channel contains three paths, including the LOS. The relative path power gains are $0, -5, -10$dB, while the relative path delays are $0, 25T_s, 50T_s$, where T_s is the BPSK symbol period. The normalized Doppler frequency is 5×10^{-3}. For the sake of avoiding the ISI, we employ an orthogonal frequency division multiplexing (OFDM) structure, where the number of subcarriers is 512 and the length of the cyclic prefix is 64. In the simulation, we assume that the channel was time-invariant during an OFDM symbol. Fig. 10 shows both the EXIT charts and the simulated trajectories of the iterative MBER beamforming receiver at $E_b/N_0=0$dB, 2dB and 4dB. All users employ a $1/2$-rate and constraint length 4 NSC code using the octal generators of $(15, 17)$.

In Fig. 10 we note that the trajectories of the iterative process obtained by Monte-Carlo simulations closely follow the EXIT curves of the receiver components and are curtailed at the crossing of the MUD's and the decoder's curves, which indicates that the EXIT chart analysis is quite accurate for the multipath fading case. Fig. 11 shows the BER performance improvements of the system using the CMMSE, RMMSE and MBER algorithms upon increasing the number of iterations. Observe that for SNRs in excess of 4dB, the simulated BER of the MBER algorithm approaches the single-user BER, which confirms the predictions of the EXIT charts. At $E_b/N_0=5$dB, the MBER beamforming receiver achieves a near-single-user
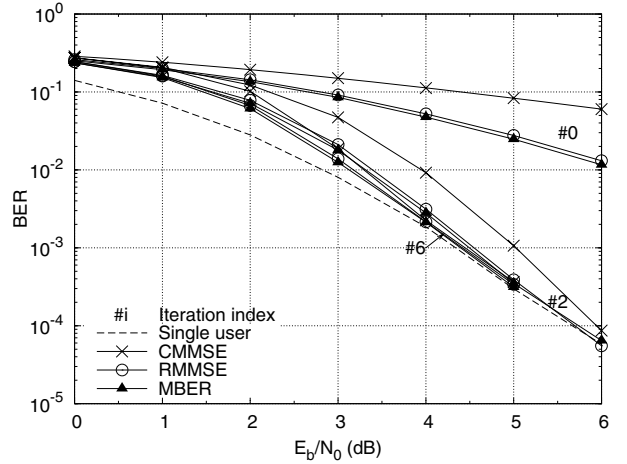
performance after two iterations, while the CMMSE and RMMSE algorithms require 6 iterations.

VI. CONCLUSION

A novel iterative MBER MUD was proposed and analysed using EXIT-charts. More explicitly, based on the EXIT charts of the SISO MUD, the exchange of extrinsic information between the multiuser detectors and the channel decoders was visualized, which facilitated their convergence analysis in the context of iterative detection. EXIT charts were also used for estimating the BER performance of the system at different user loads. Hence our results demonstrate that the EXIT chart can also be used for the analysis of the iterative MBER receiver, whose extrinsic information distribution at the MUD's output is non-Gaussian. Finally, EXIT charts were also used for comparing the convergence behaviour of various turbo receivers using different MUDs and channel codes. The turbo MBER MUD was capable of supporting $K=6$ users with the aid of two receive antennas, i.e. three times the user-load of classic beamformers.

REFERENCES

[1] J. S. Blogh and L. Hanzo, *Third Generation Systems and Intelligent Wireless Networking - Smart Antennas and Adaptive Modulation.* Chichester: John Wiley and IEEE Press, 2002.

[2] L. Hanzo, M. Münster, B. J. Choi, and T. Keller, *OFDM and MC-CDMA for Broadband Multi-User Communications, WLANs and Broadcasting.* John Wiley and IEEE Press, 2003.

[3] C. Berrou, A. Glavieux, and P. Thitimajshima, "Near Shannon limit error correcting coding and decoding: Turbo codes," in *Proc. IEEE Int. Conf. Commun.*, vol. 2, May 1993, pp. 1064-1070.

[4] L. Hanzo, T. H. Liew, and B. L. Yeap, *Turbo Coding, Turbo Equalisation and Space-Time Coding for Transmission over Fading Channels.* John Wiley and IEEE Press, 2002.

[5] L. Hanzo, C. H. Wong, and M. S. Yee, *Adaptive Wireless Transceivers: Turbo-Coded, Turbo-Equalised and Space-Time Coded TDMA, CDMA and OFDM Systems.* John Wiley and IEEE Press, 2002.

[6] L. Hanzo, L. L. Yang, E. L. Kuan, and K. Yen, *Single- and Multi-Carrier DS-CDMA: Multi-User Detection, Space-Time Spreading, Synchronisation, Standards and Networking.* John Wiley and IEEE Press, 2003.

[7] X. Wang and H. V. Poor, "Iterative (Turbo) soft interference cancellation and decoding for coded CDMA," *IEEE Trans. Commun.*, vol. 47, no. 7, pp. 1046-1060, July 1999.

[8] M. Tüchler, A. C. Singer, and R. Koetter, "Minimum mean squared error equalization using *a priori* information," *IEEE Trans. Signal Processing*, vol. 50, no. 3, pp. 673-6820, March 2002.

[9] A. Tarable, G. Montorsi, and S. Benedetto, "A linear front end for iterative soft interference cancellation and decoding in coded CDMA," *IEEE Trans. Wireless Commun.*, vol. 4, no. 2, pp. 507-518, March 2005.

[10] M. Tüchler, R. Koetter, and A. C. Singer, "Turbo equalization: principles and new results," *IEEE Trans. Commun.*, vol. 50, no. 5, pp. 754-767, May 2002.

[11] K. Li and X. Wang, "EXIT chart analysis of turbo multiuser detection," *IEEE Trans. Wireless Commun.*, vol. 4, no. 1, pp. 300-311, Jan. 2005.

[12] S. Chen, N. N. Ahmad, and L. Hanzo, "Adaptive minimum bit error rate beamforming," *IEEE Trans. Wireless Commun.*, vol. 4, no. 2, pp. 341-348, March 2005.

[13] M. Y. Alias, S. Chen, and L. Hanzo, "Multiple-antenna-aided OFDM employing genetic-algorithm-assisted minimum bit error rate multiuser detection," *IEEE Trans. Veh. Technol.*, vol. 54, no. 5, pp. 1713-1721, Sept. 2005.

[14] S. ten Brink, "Convergence of iterative decoding," *Electron. Lett.*, vol. 35, no. 13, pp. 1117-1118, June 1999.

[15] S. ten Brink, "Convergence behavior of iteratively decoded parallel concatenated codes," *IEEE Trans. Commun.*, vol. 40, pp. 1727-1737, Oct. 2001.

[16] S. ten Brink, "Designing iterative decoding schemes with the extrinsic information transfer chart," *AEÜ Int. J. Electron. Commun.*, vol. 54, pp. 389-398, Nov. 2000.

[17] R. Schober, W. H. Gerstacker, and L. Lampe, "On suboptimum receivers for DS-CDMA with BPSK modulation," *Signal Processing*, vol. 85, no. 6, pp. 1149-1163, June 2005.

[18] H. V. Poor and S. Verdú, "Probability of error in MMSE multiuser detection," *IEEE Trans. Inf. Theory*, vol. IT-43, pp. 858-871, May 1997.

[19] J. Hou, P. Siegel, and L. Milstein, "Design of multi-input multi-output systems based on low-density parity-check codes," *IEEE Trans. Commun.*, vol. 53, no. 4, pp. 601-611, Apr. 2005.

Shuang Tan received the B.E. degree and the M.E. degree in the electronic information engineering from Beijing University of Aeronautics and Astronautics, Beijing, China, in 1999 and 2002, respectively. He is currently pursuing the Ph.D. degree in ECS, University of Southampton, Southampton, U.K.

His research interests include MIMO communications, multiuser detection and iterative algorithms.

Sheng Chen (M'90-SM'97) obtained a BEng degree from the East China Petroleum Institute, Dongying, China, in 1982, and a PhD degree from the City University, London, in 1986, both in control engineering. In 2005, he was awarded DSc from the University of Southampton, Southampton, UK.

Since 1999 he has been with the School of Electronics and Computer Science, the University of Southampton, UK. He previously held research and academic appointments at the Universities of Sheffield, Edinburgh and Portsmouth, all in UK. Professor Chen's recent research works include adaptive signal processing, wireless communications, modelling and identification of nonlinear systems, neural network and machine learning, finite-precision digital controller design, evolutionary computation methods, and optimization. He has published over 280 research papers. In the database of the world's most highly cited researchers in various disciplines, compiled by Institute for Scientific Information (ISI) of the USA, Dr Chen is on the list of the highly cited researchers in the engineering category, see www.ISIHighlyCited.com

Lajos Hanzo , Fellow of the Royal Academy of Engineering (FREng), received his Master degree in electronics in 1976 and his doctorate in 1983. In 2004 he was awarded the Doctor of Sciences (DSc) degree by the University Southampton, UK. During his 29-year career in telecommunications he has held various research and academic posts in Hungary, Germany and the UK. Since 1986 he has been with the Department of Electronics and Computer Science, University of Southampton, UK, where he holds the chair in telecommunications. He has co-authored 14 John Wiley/IEEE Press books totalling about 10 000 pages on mobile radio communications and about 700 research papers, organised and chaired conference sessions, presented overview lectures and been awarded a number of distinctions. Currently he is managing an academic research team, working on a range of research projects in the field of wireless multimedia communications sponsored by industry, the Engineering and Physical Sciences Research Council (EPSRC) UK, the European IST Programme and the Mobile Virtual Centre of Excellence (VCE), UK. He is an enthusiastic supporter of industrial and academic liaison and he offers a range of industrial courses. Lajos is also an IEEE Distinguished Lecturer of both the Communications Society and the Vehicular Technology Society as well as a Fellow of both the IEEE and IEE. He is an elected Governor of the VT Society. For further information on research in progress and associated publications, please refer to http://www-mobile.ecs.soton.ac.uk